



# CHORUS

This is the accepted manuscript made available via CHORUS. The article has been published as:

## Observation of two distinct negative trions in tungsten disulfide monolayers

Abdelaziz Boulesbaa, Bing Huang, Kai Wang, Ming-Wei Lin, Masoud Mahjouri-Samani, Christopher Rouleau, Kai Xiao, Mina Yoon, Bobby Sumpter, Alexander Puretzky, and David Geohegan

Phys. Rev. B **92**, 115443 — Published 25 September 2015

DOI: [10.1103/PhysRevB.92.115443](https://doi.org/10.1103/PhysRevB.92.115443)

# Observation of Two Distinct Negative Trions in Tungsten Disulfide Monolayers

Abdelaziz Boulesbaa<sup>⊥\*</sup>, Bing Huang<sup>⊥</sup>, Kai Wang, Ming-Wei Lin, Masoud Mahjouri-Samani, Christopher Rouleau, Kai Xiao, Mina Yoon, Bobby Sumpter, Alexander Puretzy, and David Geohegan

Center for Nanophase Materials Sciences, Oak Ridge National Laboratory, 1 Bethel Valley Road, Oak Ridge, TN, 37831, USA.

<sup>⊥</sup>These authors contributed equally to this work

\*To whom correspondence should be addressed. E-mail: [boulesbaaa@ornl.gov](mailto:boulesbaaa@ornl.gov)

Ultrafast pump-probe spectroscopy of two-dimensional tungsten disulfide monolayers (2D-WS<sub>2</sub>) grown on sapphire substrates revealed two transient absorption spectral peaks that are attributed to distinct negative trions at  $\sim 2.02$  eV (T<sub>1</sub>) and  $\sim 1.98$  eV (T<sub>2</sub>). The dynamics measurements indicate that trion formation by the probe is enabled by photodoped electrons remaining after trapping of holes from excitons or free electron-hole pairs at defect sites in the crystal or on the substrate. Dynamics of the characteristic absorption bands of excitons X<sub>A</sub> and X<sub>B</sub> at  $\sim 2.03$  and  $\sim 2.40$  eV, respectively, were separately monitored and compared to the photoinduced absorption features. Selective excitation of the lowest exciton level X<sub>A</sub> using  $\lambda_{\text{pump}} < 2.4$  eV forms only trion T<sub>1</sub> implying that the electron remaining from dissociation of exciton X<sub>A</sub> is involved in the creation of this trion with a binding energy  $\sim 10$  meV with respect to X<sub>A</sub>. The absorption peak corresponding to trion T<sub>2</sub> appears when  $\lambda_{\text{pump}} > 2.4$  eV, which is just sufficient to excite exciton X<sub>B</sub>. The dynamics of trion T<sub>2</sub> formation are found to correlate with the disappearance of the bleach of X<sub>B</sub> exciton, indicating the involvement of holes participating in the bleach dynamics of exciton X<sub>B</sub>. Static electrical-doping photoabsorption measurements confirm the presence of an induced absorption peak similar to that of T<sub>2</sub>. Since the proposed trion formation process here involves exciton dissociation through hole-trapping by defects in the 2D crystal or substrate, this discovery highlights the strong role of defects in defining optical and electrical properties of 2D metal chalcogenides, which is relevant to a broad spectrum of basic science and technological applications.

## I. INTRODUCTION

A hydrogen ion composed of one proton bound to two electrons can be considered as a prototype of a negative trion [1]. Similarly, a positive trion is prototyped by a helium cation where one electron is bound to two protons [1]. In semiconductors, and particularly two-dimensional transition metal dichalcogenide monolayers (2D-TMDs), trions arise from charging bound electron-hole pairs (excitons) [2-9]. After their predicted existence in bulk semiconductors in the late 1950s [4], the journey for observing them took almost two decades [9]. With the development of confined nanostructures in the 1990s, both positive and negative trions with binding energies on the order of few meV were observed in semiconductor quantum wells [2, 3]. Since the discovery of graphene in 2004 [10], two-dimensional (2D) layered materials in general, and 2D-TMDs in particular, became a popular platform for many-body physics exploration. In fact, trions with binding energies as high as 20-40 meV were recently observed in these materials [5-8]. In 2D-TMDs, optical and electrical properties essentially arise from two intrinsic properties: the breaking of inversion symmetry and quantum confinement in one direction. For instance, the valley and spin Hall effects result due to the breaking of inversion symmetry in 2D-TMDs through the application of in-plane electric fields [11, 12]. As a result, the selection rules of optical transitions become valley dependent, which is at the heart of spintronic applications [13]. In addition, quantum confinement within monolayer thickness enhances the Coulomb interaction between holes in the valence band (VB) and electrons in the conduction band (CB). Consequently, the optical and electrical properties become dominated by excitonic effects, which makes these materials an excellent platform to explore many-body physics, contrary to bulk 3D materials where optical and electrical properties are dominated by charged free carriers [5].

Although there is a current consensus, both in the computational and experimental research communities, that in 2D-TMDs there are two band-edge exciton states  $X_A$  and  $X_B$ , only one trion state  $T_1$  has yet been observed bound by  $\sim 10\text{-}30$  meV with respect to the exciton state  $X_A$  [5, 14]. Here, through ultrafast pump-probe spectroscopy dynamics, we report the observation of two distinct trion states: a trion state  $T_1$  associated with the photoformation of exciton  $X_A$ , and a second trion state  $T_2$  observed only when pump photon energies is  $> 2.4$  eV, just sufficient to produce exciton  $X_B$ . The formations of trion states  $T_1$  and  $T_2$  are revealed in pump-probe spectroscopy as induced absorptions enabled by n-type photodoping of electrons remaining after exciton creation, and dissociation through hole-trapping at substrate or defect sites. We correlate the dynamic formation of these two trion states arising from spin-orbit splitting in the crystal. Our ultrafast pump-probe approach allows the detection of very small transient absorptions/depletions induced by the pump and the separation of different processes based on their decay dynamics, which makes possible the observation of trions with very low binding energy, even at room temperature. The results indicate that although  $X_B$  is produced through a transition between the bottom spin-orbit split (SOS) level in the valence band ( $V_2$ ) and the bottom SOS level in the conduction band ( $C_1$ ), the spectral position of the new  $T_2$  band does not correlate with that of the  $X_B$  transition ( $V_2\text{-}C_1$ ) but correlates instead to a trion state with a binding energy of  $\sim 17$  meV with respect to a ‘dark exciton’ corresponding to a transition ( $V_1\text{-}C_1$ ) that is forbidden by spin selection rules. We report that since  $T_1$  and  $T_2$  share the same  $V_1$  energy level in the VB, their formation is subject to competition dictated by the Pauli principle.

## II. METHODS

**Preparation of 2D  $WS_2$  monolayers.** Monolayers of  $WS_2$  were synthesized by low-pressure chemical vapor deposition (CVD) on sapphire substrates (crystal cut at plane [0001]) accordingly to the reported

procedure in the literature [15]. Briefly, tungsten trioxide ( $\text{WO}_3$ ) powder was placed in an alumina crucible locating the heating zone center of a two-inch horizontal tube furnace. After consecutive cleaning by acetone/isopropanol/deionized water, the substrate was also loaded downstream next to  $\text{WO}_3$  powder in the same crucible. The sulfur powder was placed in a separate crucible at the upstream side where the temperature was around  $160^\circ\text{C}$  during the growth. The furnace was heated first to  $600^\circ\text{C}$ , then  $900^\circ\text{C}$  with ramping rates of  $25^\circ\text{C}/\text{minute}$  and  $10^\circ\text{C}/\text{minute}$ , respectively. After the temperature was kept at  $900^\circ\text{C}$  for 25 minutes, the furnace was turned off and allowed to cool to room temperature. A constant  $\text{Ar}/\text{H}_2$  gas ( $\text{Ar}=60\text{ sccm}$ ,  $\text{H}_2=10\text{ sccm}$ ) was introduced into the tube furnace system and the pressure was maintained at 500 mTorr during the whole growth procedure. Similarly, monolayers of  $\text{WS}_2$  were also grown on 300 nm thick  $\text{SiO}_2$  on Si substrates with the same setup but at ambient pressure argon. The temperature of the furnace center was ramped to  $800^\circ\text{C}$  at  $20^\circ\text{C}/\text{min}$  with 50 sccm Ar, maintained at  $800^\circ\text{C}$  for 20 minutes, and then cooled down naturally with 200 sccm gas flow. To ensure a continuous sulfur vapor supply, a heating tape was used to heat the crucible containing sulfur upstream of the furnace entrance to  $120^\circ\text{C}$  during the growth.

**Simulations.** First-principles density functional theory (DFT) calculations were performed with the Vienna ab initio package (VASP) [16]. The generalized gradient approximation with the Perdew-Burke-Ernzerhof (PBE) functional for the exchange correlation potential and the projector augmented wave (PAW) method are adopted. Fourteen and six valence electrons are included for W and S potentials, respectively. The GW versions of the potentials, which are designed to provide improved scattering properties at high energies, are employed for all atoms. The kinetic energy cutoff was 500 eV. A vacuum slab of 20 Å was selected to simulate single-layer  $\text{WS}_2$ , which was sufficient to ensure minimal interlayer coupling. For Brillouin zone integration, a  $18 \times 18 \times 1$   $\Gamma$ -centered  $K$ -point mesh was used. Employing self-consistent charge density from the DFT run, we perform a subsequent non-self-consistent

spin-orbit coupling (SOC) calculation in the spirit of perturbation theory. In *GW* calculations, single-shot *GW0* calculation was performed [17] including 192 conduction bands and the energy cutoff for the response function of 300 eV. The convergence of our calculations is checked by increasing the empty bands to 384 and the *K*-point density to  $24 \times 24 \times 1$ . The BSE optical spectrum and optical transition calculations were carried out on top of *scGW*. The eight highest valence bands and the eight lowest conduction bands were included as basis for the excitonic state, which was sufficient enough to converge the energies of  $X_A$  and  $X_B$  excitonic peaks. BSE was solved using the Tamm-Dancoff approximation.

**Time-resolved spectroscopy measurements.** A home-built femtosecond pump-probe spectrometer (PPS) was used to measure ultrafast exciton dynamics in  $WS_2$  monolayers. The PPS is based on a titanium sapphire (Ti:Sa) oscillator (Micra, Coherent) with its output seeded a Ti:Sa Coherent Legend (USP-HE) amplifier operating at 1 kHz repetition rate. The Legend amplifier provides pulses centered at 800 nm, with 40 fs duration and 2.2 mJ energy per pulse. The output of the Legend amplifier was divided onto two portions: 90% was used to generate tunable excitation pulses in an optical parametric amplifier (TOPAS, Coherent), and the second portion (10%) was used to generate the white light continuum (WLC) probe in a 2 mm thick sapphire window. The WLC which covers the spectral range from 450 nm to 900 nm was collimated and focused using parabolic mirrors to minimize temporal chirp. The transmitted WLC after the sample was sent for detection through a 100  $\mu\text{m}$  core optical fiber coupled with a spectrometer-linear CCD array (USB2000ES, Ocean Optics). The pump beam was sent through a controllable optical delay-line and was chopped at 500 Hz frequency to allow absorption changes in the transmitted probe to be measured between every two successive laser shots. At every time-delay, 200 absorbance changes were averaged unless mentioned otherwise. At the sample, the probe and pump spot sizes were  $\sim 50 \mu\text{m}$  and  $\sim 100 \mu\text{m}$ , respectively. A scheme representative for the experimental setup is depicted in Fig. S1. In order to avoid photo damaging of 2D- $WS_2$  monolayers,

using one neutral density filter, the pump fluence at the sample was kept below  $2 \mu\text{J}/\text{cm}^2$ . Assuming that every absorbed photon generates one exciton, the density of generated excitons is estimated to be on the order of  $\sim 10^{11}/\text{cm}^2$ . An additional tunable neutral density filter was used to slightly adjust the intensity of excitation to produce the same maximum bleach signal size at the lowest exciton  $X_A$  upon excitation at different energies. For all excitation energies used in this work, the sample was not photodamaged based on the reproducibility of both signal size and dynamics from a scan to another, and from day to day. Additionally, it is important to note that all measurements were carried out at ambient temperature, and both pump and probe polarizations were kept linear and horizontal to the 2D- monolayer surface.

For single crystal measurements, the pump and probe beams are sent to the sample collinearly and focused down to sub-10  $\mu\text{m}$  spot sizes with a 15X reflective objective. The reflected probe is sent for detection at an Andor Newton EMCCD and Shamrock 303i Spectrograph.

**Electro-optical spectroscopy measurements.** In this experiment, a white light beam was focused with an objective microscope on a single 2D- $\text{WS}_2$  flake on silicon substrate separated by 300 nm thin layer of silica ( $\text{SiO}_2$ ). A layer of titanium (5 nm) and gold (30 nm) was deposited on the 2D- $\text{WS}_2$  in one side, and on the back side of silicon substrate. The two electrodes were connected to a Keithley 2400 source-meter. The reflected white light was focused on a slit entrance of a spectrograph (Acton Research) attached to a CCD detector (Princeton Instruments) as shown in left panel of Fig. 3. The absorbance change between absence of applied voltage ( $I_0$ ) and non-zero applied voltage ( $I_V$ ) was calculated by monitoring the intensity of the reflected light ( $I$ ) as  $\Delta A = -\log_{10} \frac{I_V}{I_0}$ .

### III. RESULTS AND DISCUSSION

Absorption spectrum of monolayer  $\text{WS}_2$  crystals grown by CVD on a sapphire substrate (Fig.S2a) shows three distinct peaks around 2.03, 2.43, and 2.91 eV superimposed on broad absorption band (Fig.

S3). Similar to bulk WS<sub>2</sub> and other transition metal dichalcogenides crystals [18]. These peaks were attributed to excitons X<sub>A</sub>, X<sub>B</sub>, and X<sub>C</sub>, respectively [5, 6, 19]. The band-edge excitons X<sub>A</sub> and X<sub>B</sub> arise from transitions between spin-orbit split levels in the valence band maximum and conduction band minimum as illustrated in Fig. 1a. For instance, at the K valley, X<sub>A</sub> (X<sub>B</sub>) is formed between a hole at V<sub>1</sub> (V<sub>2</sub>) with spin up (down) and an electron at C<sub>2</sub> (C<sub>1</sub>) with spin down (up) [8, 20, 21]. Extensive studies of the binding energies of these excitons in a monolayer WS<sub>2</sub> have been conducted using linear reflectance spectroscopy at low temperatures resulted in 0.32 eV X<sub>A</sub> binding energy [5] and two-photon photoluminescence excitation spectroscopy that gave 0.7 eV binding energy for X<sub>A</sub> exciton [6, 19]. The existing difference in the measured binding energies by different groups has been explained recently with the conclusion that these two different numbers correspond to the onsets of the band gaps of two different excitons X<sub>A</sub> (~2.4 eV) and X<sub>B</sub> (~ 2.8 eV) [22]. Theoretical attempts to explain broad absorption continuum in a similar 2D MoS<sub>2</sub> crystals showed possible large number of other strongly bound excitonic states between X<sub>B</sub> and X<sub>C</sub> broadened due to electron-phonon interaction that might explain the origin of the broad-band absorption [23]. We also calculated the energy bands and lowest excitonic transitions in 2D-WS<sub>2</sub> monolayers using GW plus Bethe-Salpeter equation (GW-BSE) (see Fig. S2b). Depicted in Fig. 1a are the four energy levels resulting from spin-orbit splitting (SOS) at the conduction band minimum (CBM) and valence band maximum (VBM) at the *K* and *K'*=-*K* points. These levels are associated with two optically active excitonic transitions X<sub>A</sub> (~ 2.03 eV) and X<sub>B</sub> (~ 2.40 eV).

To understand the dynamics of these band-edge excitons, ensembles of 3-5 μm 2D-WS<sub>2</sub> monolayer crystals were probed by femtosecond pump-probe spectroscopy. It should be noted that we used a multicrystalline monolayer WS<sub>2</sub> sample with the 50 μm-probe beam covering multiple individual crystals, including their edges and grain boundaries. Recently it has been reported that excitons from the crystal edges are red shifted (~50 meV) compared to excitons from flake centers [24]. Consequently, this



sample provides ensemble information on the position of quasiparticles absorption bands due to contributions from the flake centers and edges that lead to spectral shifts and broadening. Comparison with transient absorption measurements from the center of large ( $\sim 40 \mu\text{m}$ )  $\text{WS}_2$  single crystals grown on  $\text{SiO}_2/\text{Si}$  substrates is given in Fig. S4.

2D- $\text{WS}_2$  monolayers were excited at 2.1 eV and 3.1 eV by the pump beam, and the temporal evolutions of  $X_A$  and  $X_B$  bleach formations and recoveries were tracked by the probe pulse. Transient absorption spectra (TAS) resulting from excitation at 2.1 eV demonstrated the sub-ps formation of excitons  $X_A$  and  $X_B$  (Fig. 1b). The time required for the bleach of  $X_A$  to reach its maximum amplitude was about 500 fs longer in the case of excitation at 3.1 eV (Fig. 1c). This delay is related to the intraband relaxation from higher excited states populated with 3.1 eV pump laser to the lowest excitonic state  $X_A$ . This has been observed previously for  $\text{MoS}_2$  monolayers [25]. Fig. 1c shows that the bleach recovery of  $X_A$  was faster ( $\sim 9$  ps) in the case of 2.1 eV pump compared to that for 3.1 eV ( $\sim 22$  ps) (see Table S1). This suggests the possibility of a quenching pathway of  $X_A$  that is more efficient in the case of near resonance excitation of  $X_A$ .

To investigate the reason for the  $X_A$  bleach lifetime dependence on the excitation photon energy, TAS collected at 500 ps time-delays upon excitation at 2.1 eV and 3.1 eV were closely examined (Fig. 1d). In the case of excitation at 2.1 eV, the spectrum shows an induced absorption ( $T_1$  in Fig 1b and d) at the “red” side of  $X_A$ . The spectrum of  $T_1$  was fit well to one gaussian, but in the case of excitation at 3.1 eV, the fit of the induced absorption spectrum at 500 ps delay, required two gaussians (Fig. 1d). During the fit of this spectrum, the width and center of  $T_1$  were fixed, and the parameters of the second component ( $T_2$ ) were returned by the fit (Fig. 1d). These induced absorptions located at the “red” side of  $X_A$  may have several origins such as exciton-exciton and exciton-free carrier collisional broadening of

the excitonic absorption bands [25, 26], biexciton formation [14, 27], many-body interaction effects [27], intraband transitions [25], laser heating, neutral bound exciton trapping [28], or charge trapping [29]. However, some of these processes can be excluded based on the dynamics of these induced absorptions  $T_1$  and  $T_2$ .

In order to identify the source of  $T_1$  and  $T_2$  induced absorptions, we examine the TAS collected at early time-delays (Fig. 2). Consistent with Fig.1d,  $T_2$  induced absorption  $\sim 1.98$  eV was observed only in the case of excitation at 3.1 eV (Fig. 2a). Additionally, both sets of transient spectra contained a negative differential absorbance that indicates stimulated emission and depletion of  $X_A$ , as well as an early time-delay photoinduced absorption (XX) feature at energies  $\sim 1.94$  eV. Based on the dynamics of XX and  $T_2$  shown in Fig. 2c and d, respectively, these two features can be spectrally distinguished. In fact, XX was formed instantaneously and disappeared within  $\sim 20$  ps after excitation, but  $T_2$  was formed slowly and did not reach its maximum amplitude until 20 ps after excitation. Moreover,  $T_2$  decays slowly, with portions of its amplitude survived up to hundreds of ps, but XX decays with a 6 ps time constant, which is even faster than that of  $X_A$  bleach recovery ( $\sim 9$  ps) (see Tables S1 and S3 in the supplementary information). The XX absorption feature observed for both 2.1 eV and 3.1 eV pump excitations can be attributed to exciton-exciton and exciton-free carrier collisional broadening of the excitonic absorption bands [25] and/or biexciton formation [14].

To eliminate the possibilities of changes in the oscillator strength due to shift in excitons absorption, laser heating and free carrier generation, we carried out a control experiment. Transient absorption spectra were collected upon excitation of the same spot on the sample and under the same pump fluence ( $\sim 2 \mu\text{J}/\text{cm}^2$ ) using two pump photon energies: 2.3 eV (insufficient for  $X_B$  generation) and 2.4 eV (sufficient for  $X_B$  generation). The resulting spectra shown in Fig. S7a and b, demonstrate that  $T_2$

was observed when the pump photon excitation energy was  $\geq 2.4$  eV, which matches the position of the  $X_B$  absorption band and the possible onset of the  $X_A$  continuum [22] and was not observed for the pump at 2.3eV.

It is possible that the  $T_1$  and  $T_2$  induced absorption features indicate exciton absorption broadening shifts resulting from many-body interaction effects, such as exciton-exciton or exciton-free carriers interactions [26, 27, 30]. In strongly confined systems, the absorption spectrum of photogenerated excitons can be broadened due to Coulomb interactions arising from many-body exciton-exciton repulsive interactions [26, 27]. According to Fig. 1c, excitons ( $X_A$ ) disappeared within the first 100 ps following pump excitation; the clearly-resolved spectral features measured at 500 ps in Fig. 2d should be devoid of such exciton-exciton or exciton-free carrier interactions. Moreover, by 20 ps time-delay, more than 90% of exciton  $X_A$  bleach has recombined (see Fig. 1d), and at this same time-delay  $T_2$  amplitude was the greatest (see Fig. 2d ). If  $T_2$  originated from exciton-exciton and/or exciton-free carriers interaction, one would expect  $T_2$  amplitude to be the greatest when  $X_A$  bleach amplitude is the highest. Similar arguments apply for intraband transitions; which should also be unlikely after 20 ps time-delay.

For the possibility of bound exciton trapping, one would expect the electron and hole to recombine at most within the same time scale as  $X_A$  because both electron and hole are trapped together and still bound to each other. Transient absorption results shown in Fig. 1c and d indicate that  $X_A$  lived less than 100 ps but  $T_1$  and  $T_2$  induced absorptions survived beyond 500 ps after excitation. Consequently, this possibility of bound exciton trapping can be ruled out.

In conclusion, based upon the above dynamics analysis and the control experiment of exciting at 2.3 and 2.4 eV, it is unlikely that the processes of laser heating, bi-exciton formation, many body

interaction effects, neutral bound exciton trapping, or intraband transitions are viable explanations for the origin of the induced absorptions  $T_1$  and  $T_2$ . A much more likely scenario for the long lifetimes observed for features  $T_1$  and  $T_2$  is photoinduced absorption arising from charge trapping of electrons or holes, a process that can last hundreds of picoseconds, which is consistent with the spectra of  $T_1$  and  $T_2$  measured 500 ps after excitation as shown in Fig. 1d.

In this scenario, we hypothesize that excitons  $X_A$  and  $X_B$ , generated by the pump pulse, dissociate through transferring their holes to trapping sites (ST) that belong to the substrate or defects in the crystal, leaving their electrons in the CB to bind with electron-hole pairs generated by the probe pulse to form negative trion states (conversely, positive trion formation would involve electron trapping, and residual holes). Similar trion formation upon exciton dissociation has been observed in carbon nanotubes [29, 31].

To test the hypothesis of trions generation through charge trapping, the dependence of  $T_1$  and  $T_2$  absorption on pump laser fluence was measured at 500 ps delay. According to Fig. S5 and S8 in the Supplementary Information, while  $X_A$  and  $X_B$  depletions saturate at  $\sim 6 \mu\text{J}/\text{cm}^2$  energy fluence,  $T_1$  and  $T_2$  induced absorption features saturate at  $\sim 3 \mu\text{J}/\text{cm}^2$  pump fluences, indicating that  $T_1$  and  $T_2$  amplitudes are more correlated with the number of available trapping sites rather than the production of  $X_A$  and  $X_B$ .

If  $T_1$  and  $T_2$  reflected the generation of positive trions due to electron trap states located within the bandgap of 2D- $\text{WS}_2$  monolayers, they would be populated as long as  $X_A$  or  $X_B$  is formed. According to transient spectra shown in Fig. 1d,  $T_2$  was not observed in the case of excitation at 2.1 eV despite the fact that  $X_A$  was equally populated as in the case of excitation at 3.1 eV. Similarly, according to Fig. 1d, the amplitude of  $T_1$  resulting from excitation at 3.1 eV was only third of that occurring by excitation at 2.1 eV despite the fact that the amplitudes of the  $X_A$  bleach were the same (Fig. 1c). Consequently, it is

unlikely that  $T_1$  and  $T_2$  are positive trions that originate by optically p-doping  $WS_2$  as a consequence of trapping electrons by the substrate or defect sites. However, the alternative case where  $X_A$  and  $X_B$  undergo dissociation via holes trapping to substrate or defect sites, essentially optically doping the semiconductor n-type, excitation by the probe pulse may lead to the formation of negative trions.

To check this hypothesis we carried out electro-optical spectroscopy (EOS) measurements (Fig. 3). When introducing excess electrons into the CB upon the application of positive voltages, static absorbance change spectra (comparing bias on/off) exhibited an induced absorption similar to  $T_2$ . Furthermore, as the n-doping level increased with increasing bias, the amplitude of this feature increased. A corresponding induced absorbance similar to  $T_1$  was not observed probably due to the close spectral overlap between the positions of absorption of  $T_1$  and the bleach of  $X_A$ . Note that in the femtosecond transient measurements,  $T_1$  became observable only after the  $X_A$  bleach had completely disappeared (Fig. 1d), but in static EOS measurements, possible  $T_1$  absorbance is unresolvable due to the strong  $X_A$  bleach. It should be noted additionally, that in the EOS measurements the substrate was  $SiO_2/Si$  while in the femtosecond pump-probe experiments, the substrate was sapphire. Upon application of negative voltages, which consists of introducing excess holes into the VB, the resulting absorbance spectrum was completely different than previously measured for  $T_1$  and  $T_2$ . It contained a spectrally broad induced absorption that is different than  $T_1$  and  $T_2$  observed in Fig. 1d, which may indicate the generation of positive trion states.

Because in these experiments trions form as a result of photoabsorption involving a free electron resulting from exciton formation and dissociation, in the case of excitation at 2.1 eV,  $T_1$  should originate from photodoping resulted from dissociation of  $X_A$ . However, in the case of pumping at 3.1 eV, both  $X_A$  and  $X_B$  excitons as well as free electrons and holes are generated, which allowed the photoformation of both  $T_1$  and  $T_2$  by the probe light. Noting that the amplitude of  $T_1$  was third that using pump at 2.1 eV.

Within the framework of  $T_1$  and  $T_2$  photogeneration via holes transfer to a trapping site belonging to the substrate of defects in the crystal, the ambiguous dependence of the  $X_A$  bleach recovery dynamics on the excitation energy, observed in Fig. 1c, can be explained according to a mechanism of trion photogeneration as depicted in Fig. 4. Upon pump laser excitation at 2.1 eV, where only  $X_A$  is generated, the faster  $X_A$  bleach recovery is attributed to more efficient transfer of the  $X_A$ -hole to the trapping site, which also produced more  $T_1$ . Indeed according to Fig. 1d, the amount of generated  $T_1$  following pumping at 2.1 eV was three times of that for excitation at 3.1 eV.

Depicted in Fig. 4 is a cartoon representation for the mechanism of  $T_1$  and  $T_2$  generation in these pump-probe experiments. Upon near-resonant excitation with respect to  $X_A$ , the generated excitons dissociate via hole trapping at trapping sites on adsorbates or on the substrate, and  $T_1$  is generated as follows: the remaining electron with spin state down (up)  $|e\downarrow\rangle$  ( $|e\uparrow\rangle$ ) at the K (K') valley binds to the newly generated electron-hole pair  $|h\downarrow e\uparrow\rangle$  ( $|h\uparrow e\downarrow\rangle$ ) at the K'(K) valley upon absorption of probe photons to form  $T_1$ . Noting that this photogenerated trion  $T_1$  is in its ground state  $|h\uparrow e\downarrow e\uparrow\rangle$  [32] at the K-valley and  $|h\downarrow e\uparrow e\downarrow\rangle$  at the K'-valley. In the case of excitation with photon energies  $\geq 2.4$  eV (sufficient for  $X_B$  generation and possible production of free carriers), the  $X_B$  dissociation through hole trapping leaves a free electron  $|e\uparrow\rangle$  ( $|e\downarrow\rangle$ ) at the K (K') valley, which binds to the electron-hole pair  $|h\uparrow e\downarrow\rangle$  ( $|h\downarrow e\uparrow\rangle$ ) generated by the probe pulse to form  $T_2$  **in its ground state** at the K(K') valleys **through the trionic transition. Noting that in absence of the photodoping electron at  $C_1$ , an excitonic transition  $V_1 \rightarrow C_1$  is optically forbidden.** In this case, population of both  $C_1$  and  $C_2$  in the CB is possible, but the exclusivity of  $T_1$  and  $T_2$  photogeneration is controlled by Pauli blocking at  $V_1$  in the VB.

Although it is possible to generate  $T_2$  even upon pumping below  $X_B$  due to inter-valley spin flip [20] of  $X_A$ 's remaining electron, which crosses the valley to  $C_1$ , and can bind to electron-hole pairs

generated by the probe through the **trionic** transition across  $V_1 \rightarrow C_1$  to form  $T_2$ , we did not observe it possibly due to Pauli blocking at  $V_1$ , because this level is already occupied by the  $T_1$  hole. Also, in transient absorption spectra, one would expect to see an additional induced absorption near  $X_B$  reflecting the generation of a trion through the **trionic transition across**  $V_2 \rightarrow C_1$ . Our measurements did not indicate the formation of this trion, which is consistent with EOS experiments where even at high n-doping (see Fig. 3), no noticeable induced absorption to the red side of  $X_B$  was observed. This is in accordance with recent reports of low temperature static photoluminescence under external n-doping [6].

#### IV. CONCLUSION

In summary, ultrafast pump-probe spectroscopy of 2D- $WS_2$  monolayers identified two spectral absorption peaks that we attribute to different negative trions. The mechanisms and dynamics for their photogeneration were revealed by monitoring the characteristic absorption bands and dynamics of the two lowest excitons,  $X_A$  and  $X_B$ , for different pump laser wavelengths. Pump laser photon energies  $< 2.4$  eV sufficient to create only  $X_A$  exciton result, in a single photoinduced absorption band centered at  $\sim 2.02$  eV (25 meV FWHM) that we attribute to trion states  $T_1$ , which are bound by  $\sim 10$  meV with respect to  $X_A$ , in good agreement with reference [14]. This photoabsorption to create trions persists for  $\sim 1$  ns and correlates with the bleach recovery time of  $X_A$ , from which we conclude that free electrons that are necessary to enable trion formation likely arise from exciton dissociation, enabled by hole trapping at defect sites in the  $WS_2$  crystal or the substrate which persist for these characteristic times.

A second photoinduced absorption peak at 1.98 eV, with  $\sim 18$  meV FWHM appears when  $\lambda_{\text{pump}} > 2.4$  eV, energies that are just sufficient to excite  $X_B$  exciton, which we conclude is correlated with a second negative trion state  $T_2$ . The correlation between  $T_2$  formation dynamics and  $X_B$  bleach recovery

dynamics suggest that it can be similarly generated by the dissociation of exciton  $X_B$  (and higher excitons or free electron-hole pairs) into free electrons and trapped holes. In support of the hypothesis that the photoinduced absorbing species are negative trions forming as a consequence of n-type photodoping, a similar photoinduced absorption feature to  $T_2$  was observed by externally n-doping the sample, the amount of generated  $T_2$  increasing with increasing doping level. However, the spectral position of the  $T_2$  band is 420 meV below  $X_B$  transition ( $V_2-C_1$ ), suggesting it corresponds to a trion state with a binding energy of  $17 \pm 2.8$  meV with respect to a ‘dark exciton’ corresponding to a transition ( $V_1-C_1$ ) that is forbidden by spin selection rules.

Because the holes of  $T_1$  and  $T_2$  occupy the same valence band level ( $V_1$ ), the formation of the two trions should undergo a Pauli blocking competition process, which is consistent with our observation that  $T_1$  decreases by two thirds when  $T_2$  is formed.

These findings highlight the strong role that charge trapping sites from substrates or adsorbates can play to affect the excitonic transitions in 2D-TMD monolayers, and the formation of quasiparticles such as trions. For instance, it should be possible to control the formation and lifetime of trapped charges, and thus the time window for trion photogeneration, through selectively designing appropriate substrate architectures. The ability to adjust the photogeneration of additional optically-active band-edge excitonic states opens a new perspective for many-body physics at the fundamental science level, and it may boost 2D-TMDs based optoelectronic applications, notably photovoltaics and information technology.

## ACKNOWLEDGEMENTS

This research was conducted at the Center for Nanophase Materials Sciences, which is a DOE Office of Science User Facility. This research used resources of the National Energy Research Scientific



Computing Center, a DOE Office of Science User Facility supported by the Office of Science of the U.S. Department of Energy under Contract No. DE-AC02-05CH11231.

## REFERENCES

- [1] H.A. Bethe, E.E. Salpeter, "Quantum mechanics of one and two electron atoms", (Springer, Berlin, 1957), 154-157.
- [2] A.J. Shields, J.L. Osborne, M.Y. Simmons, M. Pepper, D.A. Ritchie, Phys. Rev. B **52**, R5523 (1995).
- [3] H. Buhmann, L. Mansouri, J. Wang, P.H. Beton, N. Mori, L. Eaves, M. Henini, M. Potemski, Phys. Rev. B **51**, 7969R (1995).
- [4] M.A. Lampert, Phys. Rev. Lett. **1**, 450 (1958).
- [5] A. Chernikov, T.C. Berkelbach, H.M. Hill, A. Rigosi, Y. Li, Ö.B. Aslan, D.R. Reichman, M.S. Hybertsen, T.F. Heinz, Phys. Rev. Lett. **113**, 076802 (2014).
- [6] Z. Ye, T. Cao, K. O'Brien, H. Zhu, X. Yin, Y. Wang, S.G. Louie, X. Zhang, Nature **513**, 214 (2014).
- [7] K.F. Mak, K. He, C. Lee, G.H. Lee, J. Hone, T.F. Heinz, S. Jie, Nat. Mater. **12**, 207 (2013).
- [8] A.M. Jones, H. Yu, N.J. Ghimire, S. Wu, G. Aivazian, J.S. Ross, B. Zhao, J. Yan, D.G. Mandrus, D. Xiao, W. Yao, X. Xu, Nat. Nanotechnol. **8**, 634 (2013).
- [9] S. Narita, M. Taniguchi, , Phys. Rev. Lett. **36**, 913 (1976).
- [10] K.S. Novoselov, A.K. Geim, S.V. Morozov, D. Jiang, Y. Zhang, S.V. Dubonos, I.V. Grigorieva, A.A. Firsov, Science **306**, 666 (2004).
- [11] D. Xiao, M.C. Chang, Q. Niu, Rev. Mod. Phys. **82**, 1959 (2010).
- [12] N. Nagaosa, J. Sinova, S. Onoda, A.H. MacDonald, N.P. Ong, Rev. Mod. Phys. **82**, 1539 (2010).
- [13] W. Yao, D. Xiao, Q. Niu, Phys. Rev. B **77**, 335406 (2008).

- [14] J. Shang, X. Shen, C. Cong, N. Peimyoo, B. Cao, M. Eginligil, T. Yu, ACS Nano **9**, 647 (2015).
- [15] Y. Zhang, Y. Zhang, Q. Ji, J. Ju, H. Yuan, J. Shi, T. Gao, D. Ma, M. Liu, Y. Chen, X. Song, H.Y. Hwang, Y. Cui, Z. Liu, ACS Nano **7**, 8963 (2013).
- [16] G. Kresse, J. Furthmuller, Comput. Mater. Sci. **6**, 15 (1996).
- [17] M. Shishkin, G. Kresse, Phys. Rev. B **74**, 035101 (2006).
- [18] J.A. Wilson, A.D. Yoffe, Adv. Phys. **18**, 193 (1969).
- [19] B. Zhu, X. Chen, X. Cui, Sci. Rep. **5**, 9218 (2015).
- [20] C.S. Mai, Y. G.; Barrette, A.; Yu, Y.; Jin, Z.; Cao, L.; Kim, K. W.; Gundogdu, K., Phys. Rev. B **90**, 041414 (2014).
- [21] J. Kang, S. Tongay, J. Zhou, J. Li, J. Wu, Appl. Phys. Lett. **102**, 012111 (2013).
- [22] T. Stroucken, S.W. Koch, "Optically bright p-excitons indicating strong Coulomb coupling in transition-metal dichalcogenides" Preprint at <http://arXiv.org/abs/1404.4238v3> (2014)..
- [23] D.Y. Qiu, F.H. da Jornada, S.G. Louie, Phys. Rev. Lett. **111**, 216805 (2013).
- [24] H.R. Gutierrez, N. Perea-Lopez, A.L. Elías, A. Berkdemir, B. Wang, R. Lv, F. Lopez-Urías, V.H. Crespi, H. Terrones, M. Terrones, Nano Lett. **13**, 3447 (2013).
- [25] H. Shi, Y. Yan, S. Bertolazzi, J. Brivio, B. Gao, A. Kis, D. Jena, H.G. Xing, L. Huang, ACS Nano **7**, 1072 (2013).
- [26] S. Sim, J. Park, J.G. Song, C. In, Y.S. Lee, H. Kim, H. Choi, Phys. Rev. B **88**, 075434 (2013).
- [27] C. Mai, A. Barrette, Y. Yu, Y.G. Semenov, K.W. Kim, L. Cao, K. Gundogdu, Nano Lett. **14**, 202 (2014).
- [28] T. Kato, T. Kaneko, ACS Nano **8**, 12777 (2014).
- [29] S.M. Santos, B. Yuma, S. Berciaud, J. Shaver, M. Gallart, P. Gilliot, L. Cognet, B. Lounis, Phys. Rev. Lett. **107**, 187401 (2011).

[30] D. Sun, Y. Rao, G. Reider, G. Chen, Y. You, L. Brezin, A.R. Harutyunyan, T.F. Heinz, *Nano Lett.* **14**, 5625 (2014).

[31] A.M. Dowgiallo, K.S. Mistry, J.C. Johnson, J.L. Blackburn, *ACS Nano* **8**, 8573 (2014).

[32] P. Michler, "Single Semiconductor Quantum Dots", (Springer, Berlin,2009), 78-81.

All the authors discussed and approved this work

Supplementary Information accompanies this paper

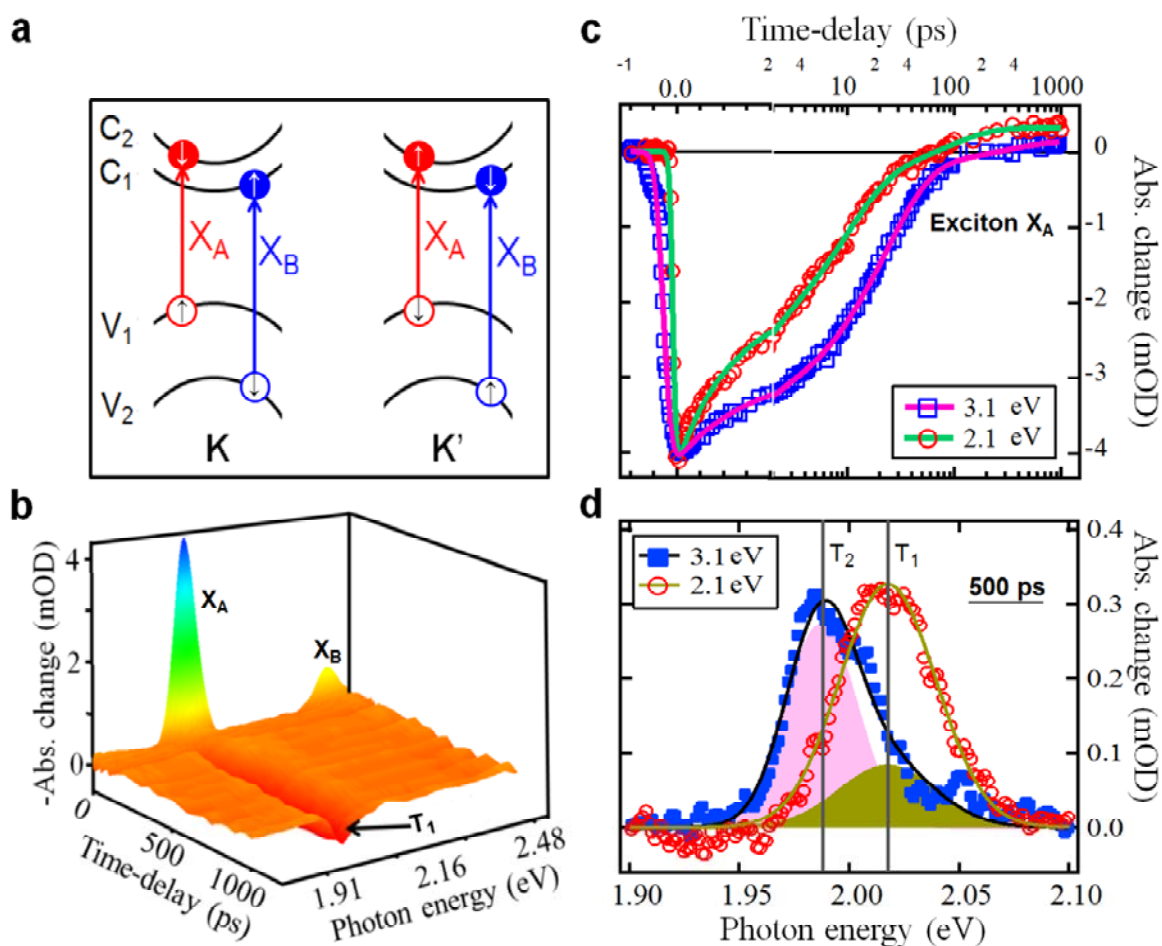


**FIG. 1. Band-edge optical transitions in 2D-WS<sub>2</sub>.** **a**, Schematic representation of the lowest excitonic transitions  $X_A$  and  $X_B$  at the  $K$ -point and  $K'=-K$  point. Spin states are indicated by small "up" and "down" arrows. **b**, Transient absorption 3-D plot upon excitation at 2.1 eV. Because 2.1 eV excitation is insufficient for  $X_B$  (2.4 eV) generation, the observed depletion of the  $X_B$  transition is due to a state-filling effect rather than generation of  $X_B$  (see Fig. S5 and corresponding supplementary text). **c**,  $X_A$  bleach dynamics upon excitation at different energies (symbols) fitted to a bi-exponential function (solid lines). One fast component describes the hot carriers relaxation, and the second component describes electron-

hole recombination. A third component to describe the positive portion of the signal was added (+0.6 and +0.2 mOD in case of 2.1 and 3.1 eV excitations, respectively). The fitting parameters are listed in Table S1. **d**, TAS recorded 500 ps after excitation as indicated. In the case of excitation at 2.1 eV, the spectrum (open circles) was fit to one Gaussian describing  $T_1$  (olive solid line). During the fit of the measured spectrum (filled squares) in the case of excitation at 3.1 eV with the sum of two Gaussians (solid dark line), the center and the width of  $T_1$  were fixed, but the center and the width of  $T_2$  were returned by the converged fit (shaded areas). The fitting parameters are listed in Table S6.

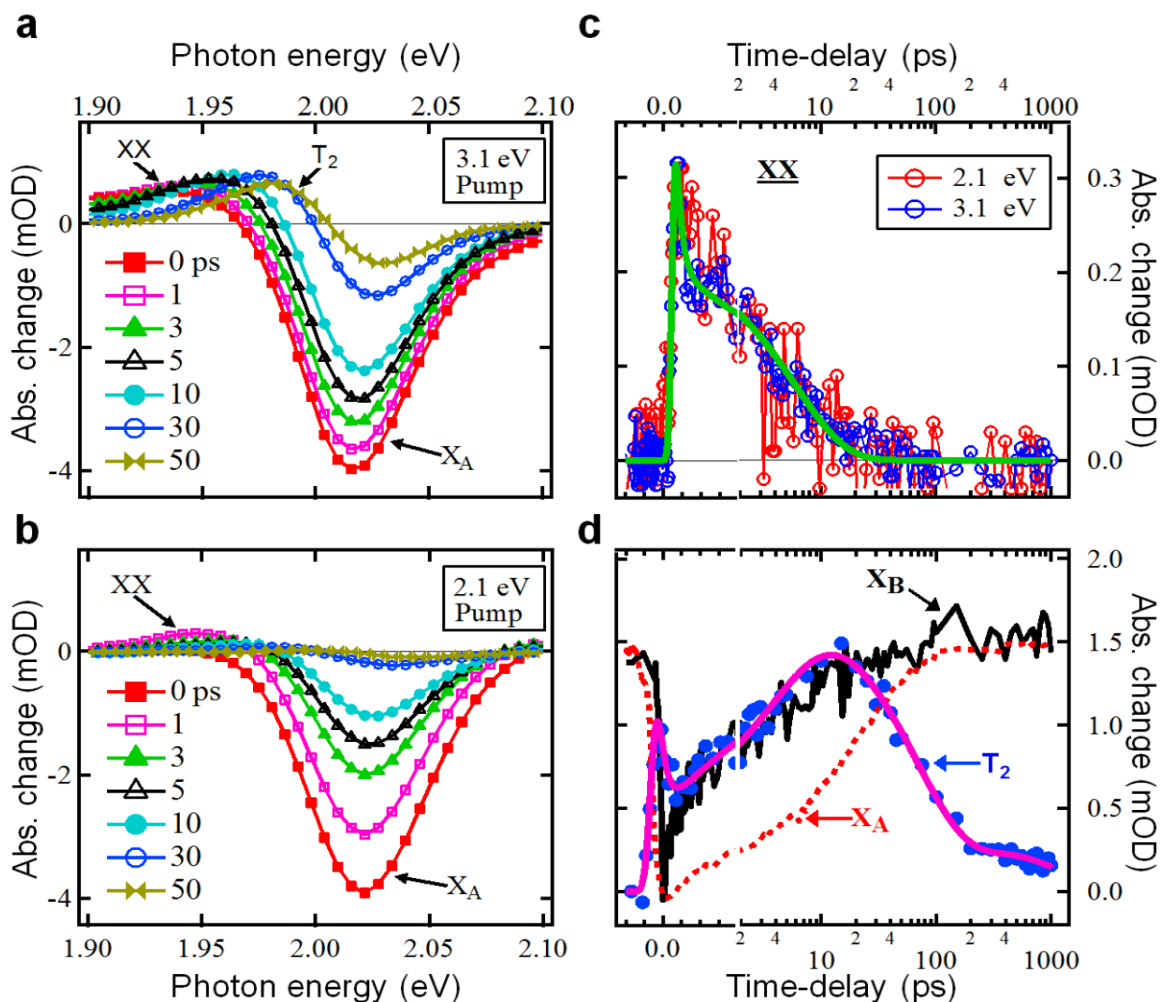


**FIG. 2. Origins of  $T_2$  and  $XX$ .** **a**, TAS collected after excitation at 3.1 eV at time-delays as indicated. **b**, TAS collected after excitation at 2.1 eV at time-delays as indicated. **c**, Dynamics of  $XX$  plotted at 1.94 eV upon excitation at 3.1 and 2.1 eV, fit to a bi-exponential function (green solid line). The fitting parameters are listed in Table S3. For clarity, the signal amplitude in the case of excitation at 3.1 eV was divided by 2 which does not affect its dynamics. **d**, Measured dynamics of  $T_2$  upon excitation at 3.1 eV plotted at 1.98 eV (filled blue circle) fit to one exponential rise (3.7 ps time constant) and two exponential decays, see Table S3 (solid pink plot). The fitting parameters are listed in Table S3. For comparison, bleach recoveries of  $X_A$  and  $X_B$  upon excitation at 3.1 eV are plotted with their amplitudes normalized and shifted to match the amplitude of  $T_2$ .

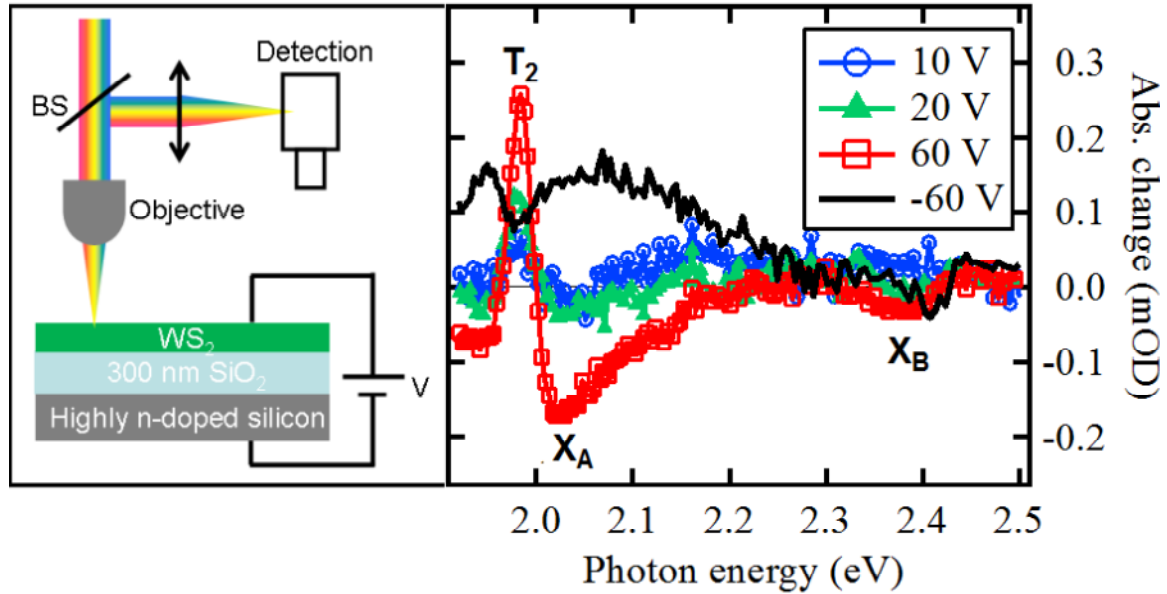


**FIG. 3.** Scheme representative for the experimental setup used for electro-optical static transient absorption measurements (left panel), and absorbance change spectra at different n-doping levels as indicated (right panel).

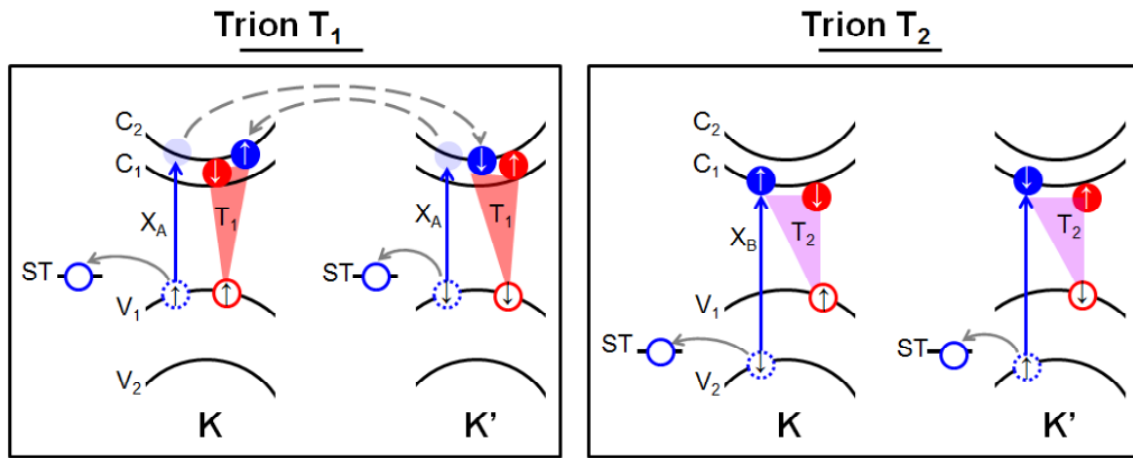


**FIG. 4. Mechanism of  $T_1$  and  $T_2$  generation at the K and K' points in a pump-probe experiment.** (Left panel) Exciton  $X_A$  (blue circles) is generated upon quasi-resonant excitation with respect to  $X_A$  by the pump pulse. Following dissociation of  $X_A$  (at both K and K') through hole trapping at the substrate or a defect site (ST), the remaining electron at the K(K') valley **joins (dashed arrows)** the newly generated electron-hole pairs (red circles) by the probe at K'(K) **to form  $T_1$** . (Right panel) Upon generation of exciton  $X_B$  (blue circles) using sufficient pump photon energy, and following its dissociation through hole trapping at ST, the remaining electron at  $C_1$  binds to the newly generated electron-hole pairs (red circles) through the  $V_1 \rightarrow C_1$  trion transition upon absorption of probe photons. **To account for  $T_1$  and  $T_2$  binding energies, they are depicted lower than  $C_2$  and  $C_1$  levels, respectively.**